Comparing surface and mid-troposphere CO_2 concentrations from central U.S grasslands

by Ferdouz V. Cochran et al.

2013

Entropy **2013**, *15*, 606-623; doi:10.3390/e15020606

OPEN ACCESS

entropy

ISSN 1099-4300

www.mdpi.com/journal/entropy

Article

Comparing Surface and Mid-Tropospheric CO_2 Concentrations from Central U.S. Grasslands

Ferdouz V. Cochran *, Nathaniel A. Brunsell and David B. Mechem

Department of Geography, University of Kansas, 1475 Jayhawk Blvd, Lawrence, KS 66045, USA; E-Mails: brunsell@ku.edu (N.A.B.); dmechem@ku.edu (D.B.M.)

* Author to whom correspondence should be addressed; E-Mail: ferdouzv@ku.edu; Tel.: +1-785-864-2021; Fax: +1-785-864-5378.

Received: 1 January 2013; in revised form: 15 January 2013 / Accepted: 29 January 2013 / Published: 6 February 2013

Abstract: Comparisons of eddy covariance (EC) tower measurements of CO_2 concentration with mid-tropospheric observations from the Atmospheric Infrared Sounder (AIRS) allow for evaluation of the rising global signal of this greenhouse gas in relation to surface carbon dynamics. Using an information theory approach combining relative entropy and wavelet multi-resolution analysis, this study has explored correlations and divergences between mid-tropospheric and surface CO_2 concentrations in grasslands of northeastern Kansas. Results show that surface CO_2 measurements at the Kansas Field Station (KFS) and the Konza Prairie Biological Stations 1B (KZU) and 4B (K4B) with different land-cover types correlate well with mid-tropospheric CO_2 in this region at the 512-day timescale between 2007 and 2010. Relative entropy further reveals that AIRS observations are indicative of surface CO_2 concentrations for all land-cover types on monthly (32-day) and longer timescales. AIRS observations are also similar to CO_2 concentrations at shorter timescales at sites KFS and K4B experiencing woody encroachment, though these results require further investigation. Differences in species composition and microclimate add to the variability of surface concentrations compared with mid-tropospheric observations.

Keywords: Atmospheric Infrared Sounder; eddy covariance; information theory; relative entropy; wavelets; Konza Prairie

1. Introduction

The distribution of carbon dioxide (CO_2) in the mid-troposphere is influenced by tropospheric weather and large-scale circulation patterns around the globe and interannual variability associated with the El Niño Southern Oscillation (ENSO) [1,2]. Areas with enhanced upward or downward motions associated with large-scale circulations can transport CO_2 between the free troposphere (FT) and the atmospheric boundary layer (ABL) on the timescale of a day [3]. If information related to CO_2 concentrations flows between synoptic systems and the ABL on a daily to subdaily timescale [3,4], changes in soil moisture, surface albedo, and temperature that drive biosphere-atmosphere interactions at short timescales may also influence mid-tropospheric CO_2. While observations of the vertically integrated CO_2 mixing ratio have been found to be influenced by continental-scale flux patterns [5], it is not yet understood how local fluxes from varying land-cover types relate to CO_2 concentrations in the mid-troposphere.

How is the high-frequency variability of CO_2 in the ABL communicated to the FT, and how do CO_2 concentrations in the FT influence CO_2 concentrations in the ABL? In contrast to ABL CO_2 concentrations, FT CO_2 concentrations are governed exclusively by transport mechanisms, either large-scale ascent or descent associated with the Hadley/Walker circulation, other large-scale cells, or baroclinic/synoptic disturbances. Cotton *et al.* [6] quantified "venting" of ABL air into the FT by cloud circulations of different scales and found that synoptic cyclones or mid-latitude baroclinic waves constitute the greatest contribution to ABL venting. One mesoscale modeling study demonstrated that 70% of passive tracers initialized in the boundary layer are transported to the free troposphere over a period of three days [7]. Sinclair *et al.* [8] attributed this substantial exchange between ABL and FT to the warm conveyor belt, which provides substantial ascent from the ABL to the mid-troposphere. A detailed mass budget demonstrates the ventilation of ABL air into the FT over the warm sector, as well as the entrainment of FT air behind the cold front and near the high-pressure center [9].

Convective circulations can also promote exchanges between the ABL and FT. Isolated shallow and deep convective cells can ventilate the boundary layer over small areas in the span of a few hours [10,11]. Mesoscale convective systems (MCS), complexes of thunderstorms characterized by an organized mesoscale circulation, provide much of the warm-season rainfall over the central U.S. [12,13], and these systems contribute substantially to the exchange of air between the ABL and FT [6]. In the case of MCSs, the exchanges are brought about by individual convective updrafts but also via coherent mesoscale flow structures associated with these systems (e.g., [14,15]). Boundary-layer venting from deep convection can also accompany synoptic systems, as in the case of embedded convective elements along a cold front [16]. Penetrative downdrafts would presumably serve as a means of injecting FT air into the ABL, but this mechanism has not been emphasized in these previous tracer and budget studies.

A recent study examining total column CO_2 finds that during a frontal system passing over the Park Falls, WI tall tower, CO_2 concentration above 5 km increased around 5 ppm while drawdown of boundary layer CO_2 decreased [5] . These observations confirm that horizontal advection and gradients play a role in total CO_2 column variation on a subdaily time scale. Advection also influences total CO_2 column up to seasonal time scales, especially at the onset of the growing season. Keppel-Aleks *et al.* [5,17] discuss a north-south gradient, which constitutes about a 4 ppm variation between 30°N and 60°N during the growing season, correlated with variations in FT potential temperature.

The concentration of CO_2 in the ABL is a function of the composition of the original air masses during ABL formation, exchanges with the land surface, and exchanges with the FT as described above, all modulated by variables like land-cover type and soil moisture. Given the role of the inversion as a filter of information between the ABL and the FT, it is important to note the physical processes that affect transport of CO_2 within the ABL. For example, horizontal transport within the ABL is estimated to move over the land surface at approximately 500 km day^{-1} and the surface area influencing the concentration of a trace gas in the ABL, such as CO_2, ranges from 10^3 to 10^5 km^2 [18]. In addition, Cotton *et al.* [6] estimate that vertical transport from convective storm processes around the globe completely replaces the air masses in the ABL approximately 90 times per year, or every four days.

Biological processes affecting CO_2 concentrations in the ABL include photosynthesis and respiration. Greater surface CO_2 concentration implies lower levels of photosynthesis and/or higher levels of respiration by plants and microbial communities. Decreased photosynthesis and increased respiration correspond with the end of the growing season and plant senescence or greater microbial activity associated with higher soil moisture and temperature as well as increased leaf litter [19]. However, on a daily timescale, entrainment of air masses from the FT and vertical transport caused by turbulent fluxes seem to have a greater influence on the early morning temporal evolution of CO_2 concentration in the ABL than plant uptake from photosynthesis [20,21].

Land use and land-management practices also influence vegetation and carbon dynamics within the ABL. Annual burning in grasslands of the Great Plains is practiced in part to control the expansion of invasive species, such as *Cornus drummondii* (roughleaf dogwood) and *Juniperus virginiana* L. (eastern red cedar). Bremer and Ham [22] found that controlled annual burning of grasslands increases carbon loss compared with biennial burning, especially at times of above average precipitation. Shrub and tree encroachment leads to increased short-term carbon storage above ground, but these pools are vulnerable to fires and changes in land use. In addition, water availability, vegetation distribution, and rooting depth are important factors in ecosystem carbon dynamics related to woody encroachment [19,23].

Variations in photosynthesis and respiration that drive the larger amplitude of diurnal and seasonal carbon cycles associated with vegetation growth and senescence within the ABL are captured by eddy covariance (EC) tower measurements [24]. In an effort to advance studies of carbon dynamics, national and international observatory networks, such as AmeriFlux, FLUXNET, and the National Ecological Observatory Network, Inc. (NEON), have been established to combine local surface measurements from over 400 EC towers worldwide [24]. Though the average footprint of towers is on the order of 1 km^2, these surface measurements have been used to up-scale CO_2 concentrations and fluxes to provide estimates of gross primary productivity (GPP) and net ecosystem exchange (NEE) on regional to continental scales [25,26]. Estimations of NEE obtained through various "top-down" and "bottom-up" approaches remain restricted by the lack of theoretical knowledge in scaling nonlinear processes related to ecosystem fluxes [27,28].

Comparisons of surface and atmospheric measurements are key to understanding CO_2 concentrations and flux dynamics within heterogeneous landscapes and complex, nonlinear processes related to carbon cycling and climate change. Satellite measurements of atmospheric CO_2 concentrations from instruments such as the Atmospheric Infrared Sounder (AIRS) need to be evaluated in relation to ecosystem fluxes to improve assessments of NEE on varying spatial scales. To uncover the relationship

between CO_2 concentrations in the mid-troposphere and at the surface, this study asks the questions: How are temporal scales of CO_2 in the mid-troposphere related to surface CO_2 fluxes in a complex, regional landscape, such as grasslands with woody encroachment in northeastern Kansas? And, to what extent can mid-tropospheric CO_2 concentrations be used as a proxy for ABL CO_2 behavior? The goals of this comparative study are to identify the dominant temporal scales of ABL-FT exchange of CO_2 in this region and to assess the utility of AIRS mid-tropospheric CO_2 measurements for illustrating local to regional source/sink dynamics.

To examine whether and when AIRS CO_2 measurements in the mid-troposphere can be used as a proxy for concentrations at the land surface below, three EC towers were selected at sites with different land-cover types in northeastern Kansas. An information theory approach combining relative entropy and wavelet multi-resolution analysis was used to examine temporal dynamics between AIRS and EC time series of CO_2 concentrations [29]. Relative entropy, defined by Vedral [30] as an "uncertainty deficit," can be a useful measure to improve our understanding of information flow, gain, and transfer in land-atmosphere interactions [29,31]. In this study, the methodology combining wavelet multi-resolution analysis with relative entropy allows us to identify the temporal scales where there is the greatest similarity or the least divergence between the probability density functions of AIRS and EC time series of CO_2 concentrations in the mid-troposphere and at the surface.

2. Methods

2.1. Grassland Sites

Surface CO_2 concentrations were evaluated from three sites with differences in land cover and data, summarized in Table 1. The Nelson Environmental Study Area (39°N, 94°W) is comprised of 560 acres within the Kansas Field Station (KFS) owned by the University of Kansas. KFS is located north of Lawrence, Kansas, in a tallgrass prairie and deciduous forest ecotone. The eddy covariance (EC) tower at this upland site is part of the AmeriFlux network and started collecting data on July 15, 2007. It is within an abandoned grassland currently dominated by C_3 grasses, such as smooth brome (*Bromus inermis* Leyss), tall fescue (*Festuca arundinacea* Schreb.), and Kentucky bluegrass (*Poa pratensis* L.). Native grasses, forbs, and woody species are also present, and the soils are fine, montmorillonitic, mesic Aquic Argiudolls. From 1987 to 2007 this area has been experiencing woody encroachment despite management and burning approximately every five years [32]. Mean annual temperature in this temperate, mid-continental climate is 13°C, and mean annual precipitation is 937 mm.

Table 1. Eddy covariance tower sites in northeastern Kansas.

Site	Features			Data		
	Dominant Veg	Topography	Management	Missing Values (%)	RMSE (ppmv)	RMSE* (ppmv)
KFS	C_3 grass/forbs	upland	5yBurn	18.57	12.9	13.9
KZU	C_4 grass	upland	1yBurn	6.43	18.9	18.8
K4B	C_4 grass/C_3 forbs	lowland	4yBurn	5.16	13.9	14.2

RMSE* after filling both EC and AIRS time series with the mean of the original time series.

The Konza Prairie Biological Station (39°N, 96°W) is a field research station on 8600 acres south of Manhattan, Kansas, jointly owned by The Nature Conservancy and Kansas State University. Konza is located within the Flint Hills region known for flint-bearing limestone layers, and soils are fine, mixed, mesic Udic Argiustolls. This area is composed of native tallgrass prairie with primarily perennial C_4 grasses, such as big bluestem (*Andropogon gerardii* Vitman), little bluestem (*A. scoparius* Michx.), and indiangrass (*Sorghastrum nutans* (L.) Nash), and other sub-dominant grasses, forbs, and woody species. The AmeriFlux eddy covariance tower, designated as tower KZU, is located on upland watershed site 1D that has been burned annually for several decades and has not been grazed for more than 30 years [22]. Data from another EC tower located on lowland watershed site 4B, a mix of C_3 forbs and C_4 grasses burned every four years to allow for woody encroachment, are also used in the analysis. The different vegetation and burning regime at this site, referred to as K4B, broaden the scope of the study by adding a third land-cover type to the comparison between surface and mid-tropospheric CO_2. Mean annual temperature for the Konza Prairie area is also 13°C. The mean annual precipitation is 835 mm, slightly less than the more eastern KFS site and characteristic of the Kansas precipitation gradient decreasing from east to west.

2.2. Eddy Covariance Towers

The eddy covariance technique is used to measure the net ecosystem exchange of CO_2 between the biosphere and the atmosphere [33]. Micrometeorological EC towers measure fluxes of energy, water vapor, and carbon dioxide covering a longitudinal length of 100–2000 m depending on sampling height and atmospheric conditions [33]. CO_2 and water vapor concentrations are measured with an open path infrared gas analyzer, and wind speeds from a sonic anemometer at 20 Hz. Data are collected by a Campbell Scientific CR 3000 Datalogger.

The data were processed following AmeriFlux standards (see [34] for details on the post-processing algorithm), including a coordinate rotation using the planar fit method [35] as well as the standard corrections for density [36] and sonic-anemometer derived estimates of temperature [37]. In addition, corrections were made for de-spiking, lag removal, and sonic temperature heat flux for humidity, sensor separation, and spectral attenuation. Daily averages of CO_2 concentration for 2007–2010 were calculated from 48 half-hour measurements in a 24-hour period for comparison with AIRS daily observations. Missing daily values for all three EC towers (18.57% at KFS; 6.43% at KZU; 5.16% at K4B) were replaced with the mean for the entire time series at each tower. This type of data filling is selected specifically for the wavelet multi-resolution analysis that does not allow for missing values. Filling the missing data with the mean of the entire time series for each site results in a more predictable effect on longer timescales versus a less predictable effect on all timescales. Because KFS is missing more data on weekly to monthly scales, the influence of data filling may be more evident on these scales than for sites KZU and K4B.

2.3. Atmospheric Infrared Sounder

The Atmospheric Infrared Sounder (AIRS) is an instrument on the polar orbiting EOS Aqua satellite at an altitude of 705 km with equatorial cross times of 1:30 AM and 1:30 PM. It was launched on

4 May 2002, with an expected on-orbit lifetime of seven years and continues to provide global, daily observations with a native resolution of 14 × 14 km. AIRS Level 2 product resolution is 3 × 3 of the native resolution, or approximately 45 × 45 km, and the CO_2 product is 2 × 2 of that with a subsequent resolution of 90 × 90 km. The AIRS Level 3 product is regridded to a spatial resolution of 2.5° longitude by 2° latitude, thus resulting in a mean concentration.

Retrievals of CO_2 are from the 15-μm, thermal infrared band and selected cloud-cleared channels, where weighting function peaks occur between 500 hPa and 300 hPa [2]. The accuracy of CO_2 retrievals has been evaluated with information theory [38] and in comparisons with transport models, aircraft flasks, and Fourier Transform Infrared Spectrometer measurements, all resulting in an accuracy of 1–2 ppmv [1,39]. An additional 1-ppmv error in CO_2 retrievals can be caused by water vapor [40].

In this study, AIRS mid-tropospheric CO_2 concentrations were compared with observed CO_2 at the surface. A time series of AIRS Level 3 daily observed CO_2 was obtained for 2007–2010 to correspond with EC tower data, 1260 days in total. The AIRS pixels that most closely cover the KFS and Konza towers were selected: 95°W, 40°N and 97.5°W, 40°N, respectively. Due to a high percentage of missing daily values (50.48% for the AIRS pixel over KFS and 47.94% for the AIRS pixel over Konza), the mean of the entire series for each pixel is used to fill in missing daily concentrations. The wavelet multi-resolution analysis does not allow for missing values, and filling the missing data with the mean of the entire time series results in a more predictable effect on longer timescales versus a less predictable effect on all timescales. However, since AIRS missing values occur on a sub-weekly timescale, it is expected that there will be some influence on the results at shorter timescales.

2.4. Relative Entropy and Wavelet Multi-resolution Analysis

Following Brunsell [29], information theory-based relative entropy combined with a wavelet multi-resolution analysis was used to examine EC and AIRS time series. Surface and mid-tropospheric signals of CO_2 concentration were quantified as a function of temporal scale and compared at each level of decomposition, corresponding to scales of 2, 4, 8, 16, 32, 64, 128, 256, 512, and 1024 days.

Wavelet multi-resolution analysis achieves a high level of localization in both the time and frequency domains through the dilation (m) and translation (n) of a "mother" wavelet (ψ), in this case a Daubechies least-asymmetric eight wavelet. The wavelet transform is found by

$$W(m,n) = \lambda_0^{-m/2} \int_{-\infty}^{\infty} f(t)\psi(\lambda_0^{-m}t - nt_0)dt \quad (1)$$

where λ_0 is the initial scale of decomposition, and the wavelet is defined by

$$\psi_{m,n}(t) = \frac{1}{\sqrt{\lambda_0^m}}\psi\left(\frac{t - nt_0\lambda_0^m}{\lambda_0^m}\right) \quad (2)$$

Wavelet multi-resolution analysis exhibits a "zoom-in" capability that allows for the identification of brief, high-frequency events and low-frequency variability in a time series [41]. Windows of localization are narrow when examining high-frequency signals and wide when looking at low-frequency signals.

At each level of decomposition, the relative contributions of one time series to another can be obtained by reconstructing the original signal following Brunsell [29]

$$f(t) = \sum_{n} \sum_{m} D_{m,n} \psi_{m,n}(t) \tag{3}$$

where $D_{m,n}$ represents the wavelet coefficients. The original time series (X) at scale m can be reconstructed from the inverse wavelet transform of $f(t)$ at scale m. The complete time series can then be reconstructed based on these scale-wise reconstructions as

$$X(t) \approx \overline{X_m(t)} + \sum_{m \geq m_0} X'_m(t) \tag{4}$$

using residual fluctuations (X') at each point t.

Wavelet subsignals or band-pass filtered renderings of EC tower and AIRS time series at each scale of decomposition were examined for temporal variations. At each temporal scale, correlation coefficients were calculated between original, undecomposed daily time series and wavelet decomposed versions of all three EC tower and corresponding AIRS time series. Correlations between wavelet decomposed versions of EC time series and wavelet decomposed versions of AIRS time series were also analyzed. A correlation of 0.2 and above, explaining at least 20% of the variance, is considered to be indicative of a physical relationship.

Information flow, gain, and transfer between land-atmosphere interactions can be quantified with information theory-based relative entropy [29,31]. Indicating the distance between the probability density functions of variables x and y, relative entropy is defined as

$$R(x, y) = \sum_{i} p_i log \left(\frac{p_i}{q_i} \right) \tag{5}$$

R is the additional amount of information needed to represent the probability density function (pdf) of p associated with x given the probability of y in bin i determined from the pdf of q.

Relative entropy can improve our understanding of surface-atmosphere interactions by identifying temporal scales where there is greatest similarity or exchange of information between time series of mid-tropospheric and surface CO_2. The relative entropy between original and wavelet decomposed versions of AIRS and EC tower observations was obtained, and the similarity or divergence between the pdfs of CO_2 concentration in the mid-troposphere versus at the surface was quantified as a function of temporal scale. Small values of relative entropy at a particular timescale signify that the pdf of the original signal is more closely approximated by the pdf of the decomposed version of the other signal at that timescale.

Relative entropy between wavelet decomposed versions of AIRS time series and wavelet decomposed versions of EC time series were also calculated. The contribution of each decomposed series to the other remains within the timescale specified. So, instead of looking at how the pdf of one time series at a particular time scale contributes to the pdf of the other time series in full, this part of the analysis examines how the pdf of one decomposed series at a particular timescale approximates the pdf of the other decomposed series within the same timescale.

3. Results

Original, daily time series of surface EC tower measurements and mid-tropospheric AIRS observations of CO_2 concentration from 2007 to 2010 over KFS, KZU, and K4B are shown in Figure 1. Brunsell *et al.* [42] have shown that, neglecting CO_2 released during burning regimes when towers are turned off, all three EC sites are net carbon sinks. AIRS time series exhibit less amplitude and seasonal variation in CO_2 concentrations than EC tower time series. Despite high missing daily values in the original AIRS time series, a linear regression of weekly averages of the AIRS time series follows the increasing global trend in atmospheric CO_2 concentrations from approximately 384 ppmv in 2007 to approximately 394 ppmv in 2010.

Figure 1. Time series of surface EC tower and mid-tropospheric AIRS observations of CO_2 concentration from 2007 to 2010 over (**a**) KFS; (**b**) KZU; and (**c**) K4B. In all panels, the black line indicates the weekly mean of the EC time series and the dark gray line indicates the weekly mean of the AIRS tower time series.

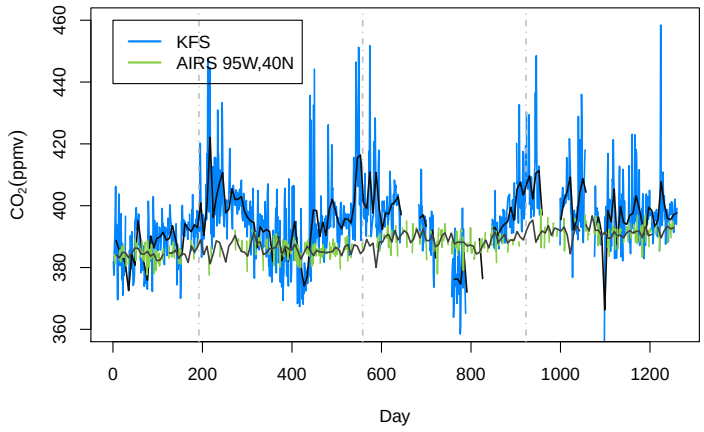

(**a**)

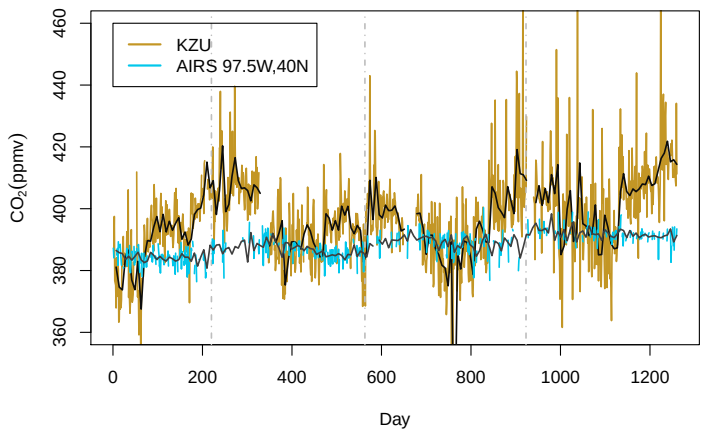

(**b**)

Figure 1. *Cont.*

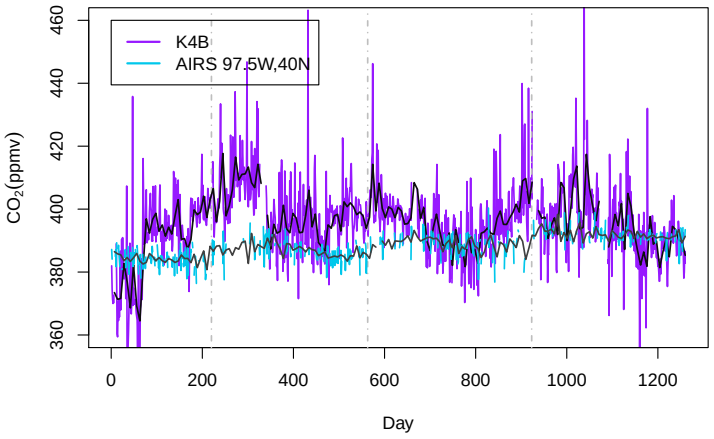

(**c**)

Root mean square error (RMSE) values between the original AIRS and EC time series show a difference of 12.9 ppmv at KFS, 18.9 ppmv at KZU, and 13.9 ppmv at K4B. Once the missing values in the time series have been replaced with the mean of each time series, the RMSE values increase to 13.9 ppmv at KFS, decrease slightly to 18.8 ppmv at KZU, and increase to 14.2 ppmv at K4B. Bias calculations show that AIRS mid-tropospheric observations exhibit a difference from surface measurements of −2.1 ppmv at KFS, −3.0 ppmv at KZU, and −3.2 ppmv at K4B before replacing missing daily values. After replacing the missing values with the mean of each time series, these biases increase to −7.6 ppmv at KFS, −8.8 ppmv at KZU, and −8.3 ppmv at K4B. The RMSE values and bias calculations indicate that site KFS and the corresponding AIRS pixel have the least difference in CO_2 concentration values. Filling missing data values increases the RMSE the most at KFS and bias calculations show an additional difference of at least 5 ppmv at all sites.

Correlations of the original time series and wavelet decompositions of the fields at each temporal scale (Figure 2) indicate that the greatest positive correlations between surface CO_2 and mid-tropospheric measurements occurs at the 512-day timescale. At correlation coefficients of 0.2 and above, wavelet decomposed versions of EC time series compared with the original AIRS time series of the corresponding pixels (Figure 2a) show that the KZU site best reflects AIRS mid-tropospheric CO_2 concentrations on a 512-day scale compared with sites KFS and K4B. The reverse relationship, where wavelet decomposed versions of AIRS are compared with the original EC time series, also highlights the 512-day scale at which mid-tropospheric CO_2 may be exchanged with the land surface at the KZU site (Figure 2b).

Comparing wavelet decomposed versions of both EC and AIRS time series (Figure 2c) reveals scales of greater contribution between surface and mid-tropospheric CO_2 exchanges. Stronger positive correlations exist at the 128-day (0.25), 256-day (0.44), and 512-day (0.61) scales for site KFS; at the 16-day (0.25) and 64-day (0.25) scales for site KZU; and at the 512-day (0.28) scale for K4B. Stronger negative correlations are seen at KFS at the 64-day (−0.43) scale, and at K4B at the 64-day

(−0.41), 128-day (−0.20), and 256-day (−0.29) scales. The very strong positive correlation (0.99) seen at the 512-day scale for site KZU is indicative of the lower reliability of longer timescales in wavelet multi-resolution analysis [43,44], especially when both time series are decomposed.

Figure 2. Correlations of (**a**) AIRS time series with wavelet decomposed versions of EC time series; (**b**) EC time series with wavelet decomposed versions of AIRS time series; and (**c**) wavelet decomposed versions of EC with wavelet decomposed versions of AIRS. Though wavelets are decomposed to ten temporal scales, only nine (corresponding to 2, 4, 8, 16, 32, 64, 128, 256, and 512 days) are shown here.

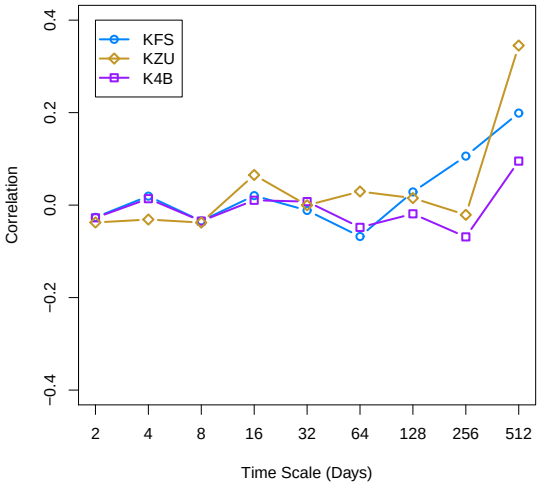

(**a**)

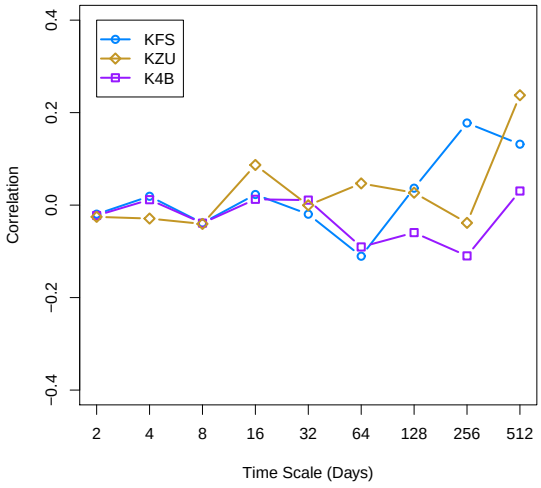

(**b**)

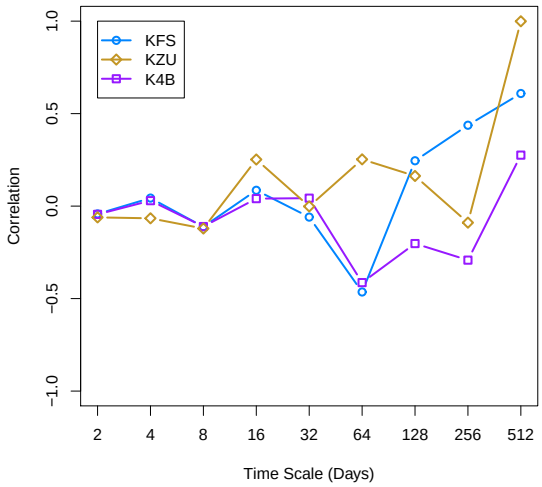

(**c**)

Relative entropy (R) of wavelet decomposed versions of the EC time series compared with the original AIRS time series, wavelet decomposed versions of the AIRS time series compared with the original EC

time series, and wavelet decomposed versions of both AIRS and EC time series are shown in Figure 3. Lower relative entropy values correspond to greater similarity between the pdfs of the time series, *i.e.*, less additional information is needed to capture the observed pdf. The timescale for which surface CO_2 concentrations are closest to the corresponding mid-tropospheric AIRS pixel varies between sites (Figure 3a). Site KFS shows the least divergence at the four-day scale ($R = 0.88$), while site KZU shows the least divergence at timescales of 32 days ($R = 0.81$) and 64 days ($R = 0.84$). K4B shows the least divergence to mid-tropospheric concentrations at the four-day to the 512-day scale, with lowest R values occurring at the four-day ($R = 0.66$), eight-day ($R = 0.84$), and 128-day ($R = 0.83$) scales.

Figure 3. Relative entropy of (**a**) AIRS time series with wavelet decomposed versions of EC time series; (**b**) EC time series with wavelet decomposed versions of AIRS time series; (**c**) wavelet decomposed versions of AIRS with wavelet decomposed versions of EC; and (**d**) wavelet decomposed versions of EC with wavelet decomposed versions of AIRS. Lower relative entropy corresponds to less divergence or greater similarity between time series.

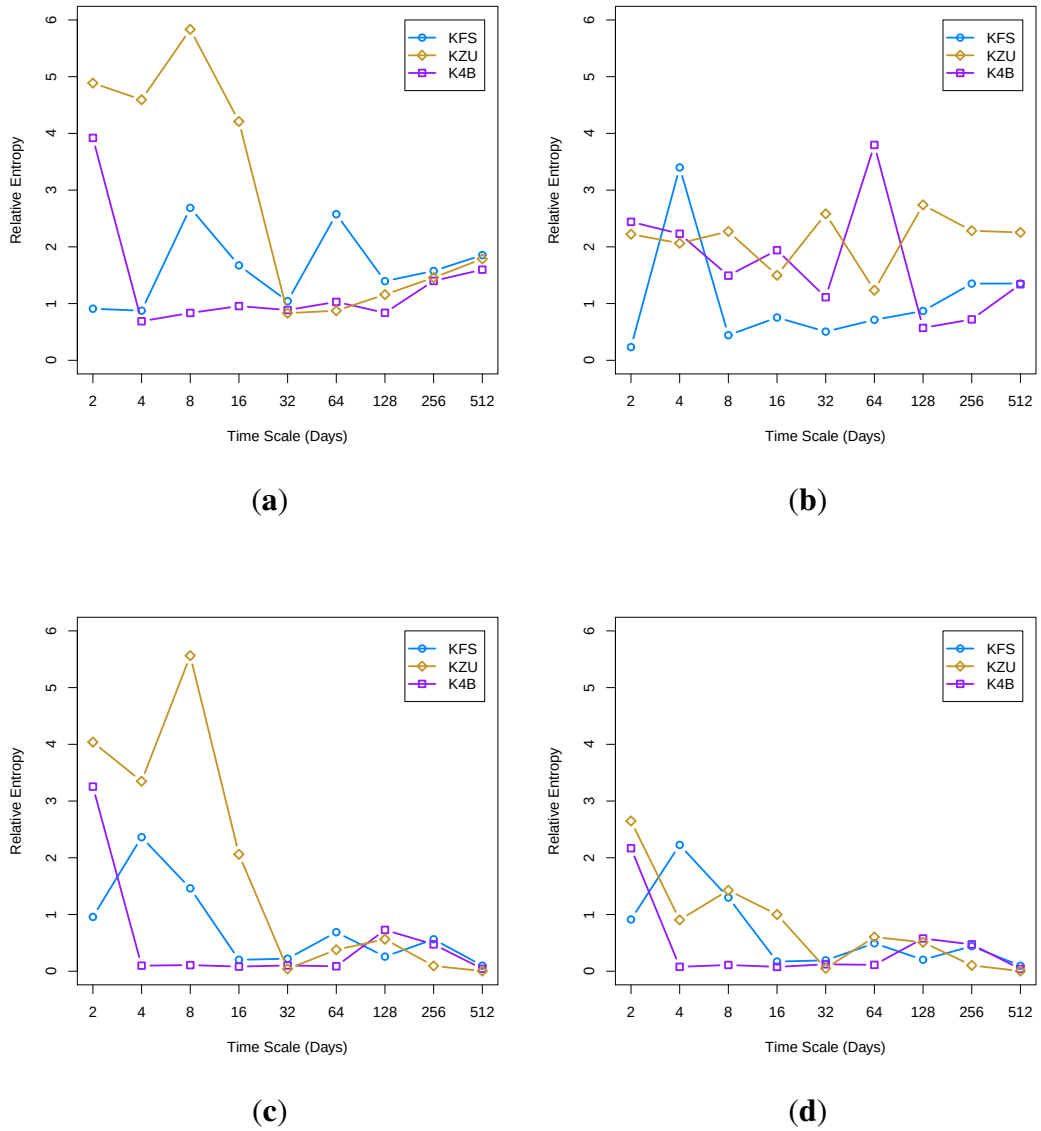

When assessing how close mid-tropospheric concentrations are to original surface EC measurements (Figure 3b), the KFS site stands out as being similar to mid-tropospheric CO_2 at all but the four-day timescale. The least divergence between mid-tropospheric CO_2 and KFS is seen at the two-day (R = 0.14) and eight-day (R = 0.44) scales, and the 16- to 512-day scales also have low R values. The lowest R values at the KZU site are seen at timescales of 16 days (R = 1.48) and 64 days (R = 1.22). The timescales of least divergence for the K4B site occur at 128 days (R = 0.52) and 256 days (R = 0.68), though R is also low at the 32- and 512-day scales.

To evaluate R between wavelet decomposed versions of both AIRS and EC time series (Figure 3c, d), the distances from pdfs of one decomposed series at a particular timescale to the pdfs of the other series at the same timescale are considered. When the distance from the pdf of the decomposed EC time series to the pdf of the decomposed AIRS time series is measured (Figure 3c), KFS shows the greatest similarity or least divergence from the 16-day (R = 0.20) to the 512-day (R = 0.10) scales; KZU shows the greatest similarity or least divergence from the 32-day (R = 0.04) to the 512-day (R = 0.003) scales; and K4B shows the greatest similarity or least divergence from the 4-day (R = 0.10) to the 512-day (R = 0.04) scales. This pattern of timescales is reflected for all sites in Figure 3d, where the distance from the pdf of the decomposed AIRS time series to the pdf of the decomposed EC time series is measured. In general, all values of R are lower when comparing series that are both decomposed.

4. Discussion

Information related to CO_2 concentration flows both to and from the land surface [4,45]. The original AIRS and EC time series show that the global signal of CO_2 concentrations in the mid-troposphere exhibits less amplitude or variation on daily to annual scales than surface concentrations (Figure 1). This finding is supported by Maddy *et al.* [39] and can be explained by the different processes governing the diurnal variability of CO_2 at the surface versus those operating between the ABL and the free troposphere (FT) to influence concentrations in the mid-troposphere [3,20].

Using an information theory-based relative entropy approach combined with wavelet multi-resolution analysis, we have identified the dominant temporal scales of ABL-FT exchange of CO_2 and of AIRS utility for revealing source/sink dynamics in this region. While correlations of the wavelet multi-resolution analysis show agreement for all sites on the 512-day timescale, the addition of relative entropy gives insight into similarities on shorter timescales. Results from relative entropy indicate that AIRS could be used as a proxy for all land cover types on the 32-day (monthly) and longer timescales. For land cover types experiencing woody encroachment like KFS and K4B, AIRS may be representative of CO_2 concentrations at shorter timescales depending on how we interpret the influences of site characterization and errors associated with missing daily values.

According to the wavelet multi-resolution analysis, the highest positive correlations between mid-tropospheric and surface CO_2 concentrations occur at 256 days for site KFS and at 512 days for sites KFS, KZU, and K4B (Figure 2). While correlations at the 512-day may be influenced by lower reliability at longer timescales in wavelet multi-resolution analysis [43,44], it is not surprising that surface and mid-tropospheric CO_2 concentrations agree on longer timescales when ABL-FT exchanges

have become more integrated. The more significant correlations for KZU at the 512-day timescale are most likely related to greater soil respiration found in annually burned grasslands, especially in years of high precipitation, as compared with sites KFS and K4B experiencing woody encroachment [22]. Ham *et al.* [46] have shown that 85% of respiration in a tallgrass prairie plot, such as KZU, can be attributed to soil respiration. A higher interannual rate of soil respiration makes KZU less of a CO_2 sink, more closely reflecting the rising global trend seen in the AIRS measurements.

Positive and negative correlations at 64 days in Figure 2c may illustrate the difference in seasonal dynamics between AIRS and the annually burned site of KZU versus sites KFS and KZU experiencing woody encroachment. Based on the findings of Keppel-Aleks *et al.* [5,17], the continental-scale gradient of CO_2, approximately 4 ppm between 30°N and 60°N, during the growing season may be related to this difference. A multi-month communication lag between ABL CO_2 and FT concentrations could manifest as a delay between the ABL carbon dynamics accompanying the onset of the growing season and the manifestation of this onset in the FT CO_2 values. This relationship between AIRS and sites KFS and K4B at the 64-day scale is also evident in the measure of relative entropy (Figure 3a & b), though the direction of information divergence is seen from KFS to AIRS (Figure 3a) and from AIRS to K4B (Figure 3b).

Results of low relative entropy for sites with different land cover types indicate timescales when AIRS is most useful for inferring source/sink dynamics at the surface (Figure 3a, c). AIRS CO_2 concentrations diverge least from surface CO_2 concentrations at site K4B, a lowland area with mixed C_4 grasses and C_3 forbs experiencing woody encroachment. Therefore, AIRS may be a good proxy for CO_2 source/sink dynamics in areas of similar land cover on timescales from 4 to 512 days. On timescales less than a month, AIRS is not a good proxy for annually-burned, C_4 grasslands like KZU.

On the other hand, Figure 3b illustrates that the CO_2 concentrations at KFS closely approximate mid-tropospheric concentrations at all but the four-day timescale. The heterogeneity and land-cover type at the KFS site is perhaps most characteristic of land cover throughout the region. For this reason, it is not surprising that EC tower measurements at KFS are closest to mid-tropospheric concentrations at almost all timescales. Likewise, it is not surprising that CO_2 concentrations at site KZU, characterized by tallgrass prairie and an annual burn regime, are the least similar with mid-tropospheric concentrations in this region. The large divergence between K4B and AIRS at the 64-day scale may again represent the seasonal differences in CO_2 concentration at local versus continental scales.

Considering that FT concentrations reflect continental-scale fluxes [5,17], it stands to reason that AIRS more closely approximates land covers with woody encroachment versus perennial tallgrass prairie. The land-cover type at site K4B, KFS, and KZU differ through species composition and microclimate. In 2008, for example, the average air temperature at K4B was found to be 0.5°C higher than the other two sites [32]. Encroachment of *Cornus drummondii* or *Juniperus virginiana* L. alters soil temperature and microclimate by changing surface albedo. The encroachment of *Juniperus virginiana* L. would also mean a change from C_4 grasses to C_3 coniferous trees. Analyses of C_3 and C_4 plants within a C_3-C_4 mixed grassland on the Konza Prairie have shown that C_3 plants with greater rooting biomass can be more drought tolerant and continue to photosynthesize beyond C_4 grasses that are drought stressed [47].

According to a study conducted on the Konza Prairie by Lett *et al.* [48], carbon storage in aboveground biomass greatly increases with shrub encroachment. Deeply rooted clonal shrub islands

of *Cornus drummondii*, characteristic of site K4B, were found to have increased from 0 to 18.5% in Konza Prairie sites burned every four years over that last 26 years [49]. These islands can sequester more than nine times the amount of carbon aboveground compared with open grasslands like KZU [48]. A shift in plant biomass from belowground to aboveground in areas of woody encroachment may cause short-term carbon sinks, though these are more vulnerable to fire and sequester less carbon as woody plants mature. In a complementary Konza Prairie study, annual soil CO_2 flux diminished by 16% as grasslands shifted to shrublands [50]. *Juniperus virginiana* L. or eastern red cedar is another invasive species found at site K4B that has been shown to alter ecosystem processes by increasing aboveground NPP, litter, and accrual of organic carbon in litter and soil, while decreasing soil respiration [51].

Various synoptic-scale and mesoscale processes couple concentrations of CO_2 in the ABL and the FT. However, attributing specific mechanisms to the correlations in the wavelet multi-resolution analysis and similarities in relative entropy is a challenge. Mechanisms governing similarities on seasonal timescales (64 to 128 days) are most obvious and straightforward to understand, since the FT CO_2 reflects the growing season over the continent, which is communicated in the vertical by regular occurrences of synoptic systems and deep convection. Relationships at shorter timescales are more difficult to interpret, partly because of the single-point nature of both the EC measurements and the AIRS pixels. A typical EC tower footprint is only 1 km^2, but we argue that measurements from a single tower are representative of a much larger regional area, given an assumption of the representativeness of the particular land-surface and vegetation properties associated with the EC measurements.

At any given moment, the bulk of the FT is composed of air that recently passed through the ABL [9], a notion consistent with the four-day cycling timescale estimated by Cotton *et al.* [6]. Similarities between AIRS measurements and both KFS and K4B sites at the four-day scale in Figure 3a are intriguing. These results may represent shorter-term communication between the ABL and FT via a small number of synoptic or organized convective systems, or they may be an artifact of the data filling process.

Given the RMSE and bias calculations, missing daily values in both the AIRS and EC time series contribute to our results and how we interpret them. Like K4B, KFS is experiencing woody encroachment, but unlike K4B the time series for KFS was originally missing 18.57% of the daily values (Table 1). Filling the missing data with the same value of the mean from the original time series may influence the results for 8- and 16-day scales shown in Figure 3a. If we disregard the higher relative entropy values for KFS at the 8- and 16-day scales, we could conclude that AIRS is also a good proxy for land-cover similar to KFS. In addition, the filling for the AIRS time series may influence the high relative entropy value on the four-day scale when the wavelet decomposed version of AIRS is compared with the original KFS signal shown in Figure 3b.

5. Conclusions

Time series of AIRS mid-tropospheric CO_2 show decreased amplitude in flux dynamics compared with surface EC measurements at sites with different land cover in northeastern Kansas. Using a combined methodology of wavelet multi-resolution analysis and the information theory approach of relative entropy, we were able to ascertain dominant temporal scales of CO_2 exchange and information gain between surface and mid-tropospheric concentrations. The greatest correlation between the surface

and mid-troposphere across all EC sites occurs at the 512-day scale, and the highest positive correlation at 256 days occurs between AIRS and site KFS experiencing woody encroachment. Relative entropy indicates that less information is needed to represent CO_2 concentrations in the mid-troposphere from measurements at the surface at 32-day and longer timescales across all land-cover types examined for the region. In sites experiencing woody encroachment, AIRS may also be representative of CO_2 concentrations at shorter timescales depending on the influences of missing daily values. Longer-term evaluation of surface and mid-tropospheric CO_2 concentrations across different land-use and land-cover types offers the potential for identifying atmospheric mechanisms, natural processes, and anthropogenic activities contributing to CO_2 source/sink dynamics, seasonal and interannual variability, and climate forcings.

Acknowledgements

This research was funded in part by the National Science Foundation EPSCoR (NSF EPS-0553722 and EPS-0919443) and KAN0061396/KAN0066263, NSF DEB-1021095, and a subcontract from the NSF Long Term Ecological Research Program at Konza Prairie Biological Station (DEB-0823341, subcontract: KAN67702). Additional funding for F.V. Cochran was provided through the IGERT C-CHANGE NSF080152 program. Thank you to the AIRS Project, NASA/JPL-Caltech, for development of the mid-tropospheric CO_2 product. Special appreciation to T. Buck and N. Wendt in the KU Biometeorology Lab for processing of the eddy covariance data. Thank you also to the two anonymous reviewers who helped improve this manuscript.

References

1. Chahine, M.T.; Chen, L.; Dimotakis, P.; Jiang, X.; Li, Q.; Olsen, E.T.; Pagano, T.; Randerson, J.; Yung, Y.L. Satellite remote sounding of mid-tropospheric CO_2. *Geophys. Res. Lett.* **2008**, *35*, L17807.
2. Jiang, X.; Chahine, M.T.; Olsen, E.T.; Chen, L.L.; Yung, Y.L. Interannual variability of mid-tropospheric CO_2 from Atmospheric Infrared Sounder. *Geophys. Res. Lett.* **2010**, *37*, L13801.
3. Li, K.-F.; Tian, B.; Waliser, D.; Yung, Y.L. Tropical Mid-Tropospheric CO_2 variability driven by the Madden-Julian oscillation. *Proc. Natl. Acad. Sci. USA* **2010**, doi: 10.1073/pnas.1008222107.
4. Ruddell, B.L.; Kumar, P. Ecohydrologic process networks: 1. Identification. *Water Resour. Res.* **2009**, *45*, W03419.
5. Keppel-Aleks, G.; Wennberg, P.O.; Washenfelder, R.A.; Wunch, D.; Schneider, T.; Toon, G.C.; Andres, R.J.; Blavier, J.F. ; Connor, B.; Davis, K.J.; *et al*. The imprint of surface fluxes and transport on variations in total column carbon dioxide. *Biogeosciences* **2012**, *9*, 875–891.
6. Cotton, W.R.; Alexander, G.D.; Hertenstein, R.; Walko, R.L.; McAnelly, R.L.; Nicholls, M. Cloud venting-a review and some new global annual estimates. *Earth-Sci. Rev.* **1995**, *39*, 169–206.
7. Kowol-Santen, J.; Beekman, M.; Schmitgen, S.; Dewey, K. Tracer analysis of transport from the boundary layer to the free troposphere. *Geophys. Res. Lett.* **2001**, *28*, 2907–2910.
8. Sinclair, V.A.; Gray, S.L.; Belcher, S.E. Boundary-layer ventilation by baroclinic life cycles. *Q. J. R. Meteorol. Soc.* **2008**, *134*, 1409–1424.

9. Sinclair, V.A.; Belcher, S.E.; Gray, S.L. Synoptic controls on boundary-layer characteristics. *Bound-Lay. Meteorol.* **2010**, *134*, 387–409.
10. Gimson, N.R. Pollution transport by convective clouds in a mesoscale model. *Q. J. R. Meteorol. Soc.* **1997**, *123*, 1805–1828.
11. Dacrew, H.F.; Gray, S.L.; Belcher, S.E. A case study of boundary-layer ventilation by convection and coastal processes. *J. Geophys. Res.* **2007**, doi: 10.1029/2006JD007984.
12. Fritsch, J.M.; Kane, R.J.; Chelius, C.R. Contribution of mesoscale convective weather systems to the warm season precipitation in the United States. *J. Appl. Meteorol.* **1986**, *25*, 1333–1345.
13. Ashley, W.S.; Monte, T.L.; Dixon, P.G.; Trotter, S.L.; Powell, E.J.; Durkee, J.D.; Grundstein, A.J. Distribution of mesoscale convective complex rainfall in the United States. *Mon. Wea. Rev.* **2003**, *131*, 3003–3017.
14. Moncrieff, M.W. A theory of organized steady convection and its transport properties. *Q. J. R. Meteorol. Soc.* **1981**, *107*, 29–50.
15. Moncrieff, M.W. Organized convective systems: Archetypal dynamical models, mass and momentum flux theory, and parameterization. *Q. J. R. Meteorol. Soc.* **1992**, *118*, 819–850.
16. Purvis, R.M.; Lewis, A.C.; Carney, R.A.; McQuaid, J.B.; Arnold, S.R.; Methven, J.; Barjat, H.; Dewey, K.; Kent, J.; Monks, P.S.; *et al.* Rapid uplift of nonmethane hydrocarbons in a cold front over central Europe. *J. Geophys. Res.* **2003**, doi:10.1029/2002JD002521.
17. Keppel-Aleks, G.; Wennberg, P.O.; Schneider, T. Sources of variations in total column carbon dioxide. *Atmos. Chem. Phys.* **2011**, *11*, 3581–3593.
18. Styles, J.M.; Raupach, M.R.; Farquhar, G.D. ; Kolle, O.; Lawton, K.A.; Brand, W.A.; Werner, R.A.; Jordan, A.; Schulze, E.-D.; Shibistova, O.; *et al.* Soil and canopy CO_2, $13CO_2$, H_2O and sensible heat flux partitions in a forest canopy inferred from concentration measurements. *Tellus B* **2002**, *54*, 655–676.
19. Scott, R.L.; Huxman, T.E.; Williams, D.G.; Goodrich, D.C. Ecohydrological impacts of woody-plant encroachment: Seasonal patterns of water and carbon dioxide exchange within a semiarid riparian environment. *Glob. Change Biol.* **2006**, *12*, 311–324.
20. Casso-Torralba, P.; Vilà-Guerau de Arellano, J.; Bosveld, F.; Soler, M.R.; Vermeulen, A.; Werner, C.; Moors, E. Diurnal and vertical variability of the sensible heat and carbon dioxide budgets in the atmospheric surface layer. *J. Geophys. Res.* **2008**, *113*, D12119.
21. Gibert, F.; Schmidt, M.; Cuesta, J.; Ciais, P. Retrieval of average CO_2 fluxes by combining in situ CO_2 measurements and backscatter lidar information. *J. Geophys. Res.* **2007**, *112*, D10301, doi:10.1029/2006JD008190.
22. Bremer, D.J.; Ham, J.M. Net carbon fluxes over burned and unburned native tallgrass prairie. *Rangeland Ecol. Manag.* **2010**, *63*, 72–81.
23. Potts, D.L.; Huxman, T.E.; Scott, R.L.; Williams, D.G.; Goodrich, D.C. The sensitivity of ecosystem carbon exchange to seasonal precipitation and woody plant encroachment. *Oecologia* **2006**, *150*, 453–463.
24. Baldocchi, D. "Breathing" of the terrestrial biosphere: Lessons learned from a global network of carbon dioxide flux measurement systems. *Aust. J. Bot.* **2008**, *56*, 1–26.

25. Xiao, J.Q.; Zhuang, B.E.; Law, D.D.; Baldocchi, J.; Chen, A.D.; Richardson, J.M.; Melillo, K.J.; Davis, D.Y.; Hollinger, S.; Wharton, R.; *et al*. Torn. Assessing net ecosystem carbon exchange of U.S. terrestrial ecosystems by integrating eddy covariance flux measurements and satellite observations. *Agric. For. Meteorol.* **2011**, *151*, 60–69.
26. Jung, M.; Reichstein, M.; Bondeau, A. Towards global empirical upscaling of FLUXNET eddy covariance observations: Validation of a model tree ensemble approach using a biosphere model. *Biogeosciences* **2009**, *6*, 2001–2013.
27. Lai, C.T.; Schauer, A.J.; Owensby, C.; Ham, J.M.; Helliker, B.; Tans, P.P.; Ehleringer, J.R. Regional CO_2 fluxes inferred from mixing ratio measurements: estimates from flask air samples in central Kansas, USA. *Tellus B* **2006**, *58*, 523–536.
28. Peters, W.; Miller, J.B.; Whitaker, J.; Denning, A.S.; Hirsch, A.; Krol, M.C.; Zupanski, D.; Bruhwiler, L.; Tans, P.P. An ensemble data assimilation system to estimate CO_2 surface fluxes from atmospheric trace gas observations. *J. Geophys. Res.* **2005**, *110*, D24304.
29. Brunsell, N.A. A multiscale information theory approach to assess spatial–temporal variability of daily precipitation. *J. Hydrol.* **2010**, *385*, 165–172.
30. Vedral, V. The role of relative entropy in quantum information theory. *Rev. Mod. Phys.* **2002**, *74*, 197–234.
31. Brunsell, N.A.; Young, C.B. Land surface response to precipitation events using MODIS and NEXRAD data. *Int. J. Remote Sens.* **2008**, *29*, 1965–1982.
32. Brunsell, N.A.; Schymanski, S.J.; Kleidon, A. Quantifying the thermodynamic entropy budget of the land surface: Is this useful? *Earth Syst. Dyn.* **2011**, *2*, 87–103.
33. Baldocchi, D.; Falge, E.; Gu, L.; Olson, R.; Hollinger, D.; Running, S.; Anthoni, P.; Davis, K.; Evans, R. FLUXNET: A new tool to study the temporal and spatial variability of ecosystem-scale carbon dioxide, water vapor, and energy flux densities. *Bull. Am. Meteorol. Soc.* **2001**, *82*, 2415–2434.
34. Baum, K.; Ham, J.; Brunsell, N.; Coyne, P. Surface boundary layer of cattle feedlots: Implications for air emissions measurements. *Agric. For. Meteorol.* **2008**, *148*, 1882–1893.
35. Wilczak, J.M.; Oncley, S.P.; Stage, S.A. Sonic anemometer tilt correction algorithms. *Bound.-Layer Meteorol.* **2001**, *99*, 127–150.
36. Webb, E.; Pearman, G.; Leuning, R. Correction of flux for density effects due to heat and water vapour transfer. *Q. J. R. Meteorol. Soc.* **1980**, *106*, 85–100.
37. Schotanus, P.; Niewstadt, F.T.M.; de Bruin, H.A. Temperature measurement with a sonic anemometer and its application to heat and moisture fluxes. *Bound.-Layer Meteorol.* **1983**, *26*, 81–93.
38. Engelen, R.J.; McNally, A.P. Estimating atmospheric CO_2 from advanced infrared satellite radiances within an operational 4D-Var data assimilation system: Methodology and first results. *J. Geophys. Res.* **2004**, *110*, D18305.
39. Maddy, E.S.; Barnet, C.D.; Goldberg, M.; Sweeney, C.; Liu, X. CO_2 retrievals from the Atmospheric Infrared Sounder: Methodology and validation. *J. Geophys. Res.* **2008**, *113*, D11301.

40. Chahine, M.; Barnet, C.; Olsen, E.T.; Chen, L.; Maddy, E. On the determination of atmospheric minor gases by the method of vanishing partial derivatives with application to CO_2. *Geophys. Res. Lett.* **2005**, *32*, L22803.
41. Lau, K.M.; Weng, H. Climate signal detection using wavelet transform: How to make a time series sing. *Bull. Am. Meteorol. Soc.* **1995**, *76*, 2391–2402.
42. Brunsell, N.A.; Nippert, J.B.; Buck, T.L. The impact of seasonality and surface heterogeneity on water use efficiency in mesic grasslands. *Ecohydrology* **2012**, submitted for publication.
43. Torrence, C.; Compo, G.P. A practical guide to wavelet analysis. *Bull. Am. Meteorol. Soc.* **1998**, *79*, 61–78.
44. Percival, D.P. On Estimation of the wavelet variance. *Biometrika* **1995**, *82*, 619–631.
45. Entekhabi, D.; Rodriguez-Iturbe, I.; Castelli, F. Mutual interaction of soil moisture state and atmospheric processes. *J. Hydrol.* **1996**, *184*, 3–17.
46. Ham, J.M.; Owensby, C.E.; Coyne, P.I.; Bremer, D.J. Fluxes of CO_2, and water vapor from a prairie ecosystem exposed to ambient and elevated atmospheric CO_2. *Agric. For. Meteorol.* **1995**, *77*, 73–93.
47. Lai, C.-T.; Schauer, A.J.; Owensby, C.; Ham, J.M.; Ehleringer, J. Isotopic air sampling in a tallgrass prairie to partition net ecosystem CO_2 exchange. *J. Geophys. Res.* **2003**, *108*, 4566.
48. Lett, M.; Knapp, A.; Briggs, J.; Blair, J. Influence of shrub encroachment on aboveground net primary productivity and carbon and nitrogen pools in a mesic grassland. *Can. J. Bot.* **2004**, *82*, 1363–1370.
49. Ratajczak, Z.; Nippert, J.B.; Hartman, J.C.; Ocheltree, T.W. Positive feedbacks amplify rates of woody encroachment in mesic tallgrass prairie. *Ecosphere* **2011**, *2*, 121.
50. McCarron, J.K.; Knapp, A.K.; Blair, J.M. Soil C and N responses to woody plant expansion in a mesic grassland. *Plant Soil* **2003**, *257*, 183–192.
51. McKinley, D.C.; Blair, J.M. Woody plant encroachment by juniperus virginiana in a mesic native grassland promotes rapid carbon and nitrogen accrual. *Ecosystems* **2008**, *11*, 454–468.